Nanoscale

PAPER

View Article Online
View Journal | View Issue

Cite this: *Nanoscale*, 2025, **17**, 16848

Effect of γ-irradiation on hexagonal boron nitride membranes and printed films†

Jingjing Wang,[a] Towseef I. Ahmad,[a] William Lee,[b] Benjamen P. Reed,[b] Yashoda Abeykoon,[a] Khaled Parvez,[a] Zixing Peng,[a] Andrew J. Pollard,[b] Aliaksandr Baidak,[c] Jordan Knapp[d] and Cinzia Casiraghi *[a,e]

Received 15th April 2025,
Accepted 17th June 2025

DOI: 10.1039/d5nr01542a

rsc.li/nanoscale

Liquid phase exfoliation (LPE) enables cost-effective and scalable production of two-dimensional (2D) materials that are suitable for fabrication of protection films and barrier coatings, through simple and low-cost techniques. Amongst 2D materials, hexagonal boron nitride (hBN) is very attractive for these applications due to its exceptional thermal and chemical stability. However, use of hBN coatings and films in environments such as reactor inspection, spent nuclear fuel handling, reprocessing facilities, or spacecraft components, which often involve elevated temperatures and/or the presence of reactive chemical species, require the protective coatings to retain their chemical, mechanical, or thermal performance under prolonged radiation exposure. In this study, we investigate the radiation tolerance to γ-rays of printed hBN films fabricated by inkjet printing and membranes produced by vacuum filtration, up to a total absorbed dose of 1500 kGy in different atmospheric conditions. Raman spectroscopy and X-ray photoelectron spectroscopy (XPS) reveal no significant structural differences in the samples up to the maximum absorbed dose, indicating excellent radiation tolerance under the conditions tested. Additionally, we did not observe structural changes in the irradiated hBN films even after prolonged exposure to air for two months. The exceptional radiation tolerance and environmental stability of the printed hBN films and membrane make them attractive as protective coatings or insulating layers in various advanced technologies for the nuclear and aerospace sectors, where long-term material stability to γ-rays is crucial.

1. Introduction

2D materials have distinct physical and chemical properties that make them attractive for a wide range of applications.[1,2] Amongst them, hBN is a very attractive material for applications in the nuclear and space industries due to its chemical inertness, high thermal conductivity and mechanical strength, as well as insulating nature.[3–6] Furthermore, hBN offers potential selectivity toward different types of radiation, due to the high thermal neutron capture cross-section of the constituent ^{10}B atoms (20% abundance) as opposed to the low cross-section for γ-rays.[7] This makes hBN an obvious candidate material for thin films and coatings used for anticorrosion, thermal management, barrier and protection. In environments such as reactor inspection, spent nuclear fuel handling, reprocessing facilities, or spacecraft components, materials are exposed to mixed radiation fields that may include γ-rays, neutrons, alpha particles, and even heavy ions. These environments also involve additional stressors, such as elevated temperatures or the presence of reactive chemical species. Therefore, protective coatings used in such scenarios must retain their chemical, mechanical, or thermal performance even under prolonged radiation exposure. While a large amount of studies has been dedicated to γ-rays irradiation of graphene and related materials, only very few studies have focussed on hBN nanocrystals[8] or composites.[9] Additionally, few-layer hBN (thicknesses between 1.6 nm and 20 nm) were used as a substrate and/or encapsulation layer for graphene field effect transistors with the aim to study the electrical response of the device after exposure to γ-irradiation.[10]

Practical applications of hBN in devices and coatings are likely to make use of films made of solution processed hBN deposited with low-cost and scalable approaches, such as printing technologies. These films are very different from bulk crys-

[a]*Department of Chemistry, University of Manchester, Manchester, M139PL, UK. E-mail: cinzia.casiraghi@manchester.ac.uk*
[b]*National Physical Laboratory, Teddington, Middlesex, TW11 0LW, UK*
[c]*Dalton Cumbrian Facility, Westlakes Science and Technology Park, CA24 3HA, UK*
[d]*United Kingdom National Nuclear Laboratory, Stonehouse Park, Sperry Way, Stonehouse, UK*
[e]*National Graphene Institute, University of Manchester, Manchester, M139PL, , UK*

†Electronic supplementary information (ESI) available: Representative Raman spectra of all samples and further data on Raman and XPS analysis. See DOI: https://doi.org/10.1039/d5nr01542a

tals and few layers, as they are made by the random assembly of hBN nanosheets with a large distribution in size and thickness, hence they consist of networks of disordered arrays of nanosheets, with a variable amount of porosity, owing to their non-perfect in-plane alignment of each nanosheet.[11] Furthermore, residual solvent and additives used to formulate the ink are adsorbed onto the nanosheets and difficult to remove completely, even after annealing, and therefore this organic residual is also expected to interact with the γ-rays, possibly contributing to changes in the properties of the overall film. Furthermore, depending on the printing technique, the film porosity, residual amount and thickness can vary dramatically.[12] Hence, the effect of γ-irradiation can lead to completely different results in printed films made of solution-processed hBN, as compared to hBN bulk crystals and single-crystal nanosheets.

This work investigates the γ-ray radiation tolerance of films made by solution-processed hBN nanosheets, produced by LPE in water with the assistance of pyrene derivatives.[13,14] Films of hBN with thickness between ~200 and 800 nm have been deposited by ink-jet printing on silicon wafers and irradiated in water-free atmospheres. In addition, thick hBN membranes (thickness >1 μm) were produced by vacuum filtration and irradiated in humid conditions. Vacuum filtration was selected to achieve thick films to minimize any effect coming from the substrate, which is also irradiated and can therefore indirectly contribute to the radiolysis of the printed film *via* charge transfer.

The samples were characterized by Raman spectroscopy and XPS before and after irradiation. Our results show no significant changes in the characteristic signals of hBN up to the highest absorbed dose of 1500 kGy, indicating that no substantial changes occurred in the structure, following the radiation exposure, making them a very attractive solution for the aerospace and nuclear sectors. This excellent resistance to γ-irradiation could be either due to the intrinsic properties of hBN or to the residual organic solvent, which could serve as "sacrificial lamb" to radiolytic degradation, either by radicals trapping and/or energy/charge transfer from the irradiated hBN nanosheets to the organic impurities.

Studying the effects of individual radiation types, such as γ-rays, is a well-established and necessary approach to understanding radiation-induced degradation mechanisms in a controlled and systematic way. Our work addresses a current knowledge gap by isolating the effect of γ-irradiation on hBN films. This serves as a foundational study to assess whether hBN is a viable candidate material for applications in more complex radiation environments.

2. Experimental

2.1 Materials

1-Pyrenesulfonic acid sodium salt (PS1), acetone, 2-propanol (IPA) and powders of hBN were purchased from Sigma Aldrich and used as-received. Type 1 deionised water (DI) was dispensed from a Millipore Directe-Q® 3UV water purification system with a resistivity of 18.2 MΩ cm at room temperature. Silicon wafers with an oxide layer (Si/SiO_2) with thickness of 90 nm, resistivity in the range of 0.001–0.005 Ω cm, a total wafer thickness of 525 μm, and as n-doping, were purchased from IDB Technologies Ltd.

2.2 Film preparation and characterization

Preparation of the hBN dispersion. The ink preparation is described in detail in previous works.[13,15] In short, the DI water was first degassed at 100 °C for 15 min and cooled down to room temperature under nitrogen. Then, 250 mL DI water, 0.25 g PS1 and 0.75 g hBN powder were placed in a glass bottle, and the dispersion was sonicated at 300 W using a Hilsonic bath sonicator for 120 hours (5 days). The resulting dispersion was centrifuged using a Sigma 1-14k refrigerated centrifuge at 3500 rpm (903*g*) for 20 minutes before collecting the supernatant. The collected supernatant was then centrifuged at 15 000 rpm (16 600*g*) for 1 hour and the precipitate redispersed in the printing solvent.[13] The dispersion was diluted to reach a concentration of 2 mg mL^{-1}, as measured by absorption spectroscopy with a PerkinElmer l-900 UV-vis-NIR spectrophotometer and by using an absorption coefficient of 1000 L g^{-1} m^{-1} (measured at 550 nm).[15] No aggregation is observed when the material is transferred into the cartridge or during printing. The resulting nanosheets have average lateral size of 160 nm and average thickness of 6.5 nm,[16] indicating an average number of layers of 6–7 (the thickness of a single-layer is ~1 nm due to residual molecules adsorbed onto the nanosheet).[17] The residual pyrene amount is below 10 wt%[18] and the nanosheets have high crystallinity, as observed by electron microscopy.[16]

Preparation of the hBN membranes. A cellulose-based filter (Whatman, qualitative filter paper, grade 1 circles, diameter of 55 mm) was used to prepare a thick membrane using 30 mL of hBN ink at a concentration of 1.0 mg mL^{-1}. The hBN dispersion was passed through the filter until all the hBN is deposited onto the membrane. The sample was then dried in air and at room temperature without any further treatment. Once dried, the membrane samples were cut into 10 mm wide segments.

Inkjet printing. A Dimatix DMP-2800 inkjet printer (Fujifilm Dimatix, Inc., Santa Clara, USA) was used to print the hBN ink onto the Si/SiO_2 substrates. Prior to printing, the substrates (65 mm × 10 mm) were cleaned with acetone then IPA for 15 minutes each, using a bath sonicator. The as-cleaned substrates were then treated with Ar plasma (Diener Electronic, Pico PCCE) for 15s to improve the wetting of the water-based hBN ink. The ink-jet printing of the hBN ink was performed using a 16 nozzle cartridge with 21.5 μm nozzle diameter and a typical droplet volume of 10 pL. The printer platen was heated to 40 °C and a drop spacing of 35 μm with a jetting voltage of 26 V was utilised. The hBN ink was used to print lines (with size of 10 mm × 0.5 mm) onto the silicon substrate with different thickness, obtained by changing the print passes (PPs).

Optical microscopy. A Nikon Eclipse LV100 microscope with a Nikon Digital Sight DS-Vi1 camera attachment was used to take optical pictures. All images were captured using a 5× objective lens, using the NIS Elements software (Version 4.30).

Profilometry. A Dektak XT profilometer was used to determine the thickness of the printed hBN films on the silicon substrate. Line scans were taken to obtain the thickness of the films, the thickness data and the root mean square (RMS) roughness was extracted using the Vision software.

Raman spectroscopy. Raman spectroscopy was performed with a Renishaw inVia Reflex Raman spectrometer equipped with a laser operating at an excitation wavelength of 325 nm. The measurements were made with a 40× objective lens and with a 2400 grooves per mm grating, using ~1.2 mW laser power on the sample. A total of five spectra were measured for each membrane and printed film in different points of the sample. The Raman measurements in the C-region (1500–1700 cm^{-1}) were conducted using a laser power on the sample significantly below 1 mW to avoid any change in structure caused by the laser illumination, which is commonly observed in disordered carbons.[19]

Following the acquisition, baseline subtraction was applied and then each Raman peak was fitted using a Lorentzian lineshape to extract the Raman fit parameters, including peak position and full width at half maximum (FWHM) of the hBN peak. The spectral resolution is 2–3 cm^{-1}.

X-Ray photoelectron spectroscopy. Selected membranes obtained by vacuum filtration were used for XPS measurements. These were carried out in ultra-high vacuum using a Kratos AXIS Supra$^+$ instrument. A monochromated aluminium X-ray source was operated at 75 W (15 kV anode voltage, 5 mA emission). The electrostatic and magnetic lens system was operated in the 'hybrid' mode with a 'slot' aperture defining an analysis area of approximately 700 μm × 300 μm on the samples. Three analysis locations were measured on each sample. The incident X-rays were at an angle of 54.7° (*i.e.* the 'magic' angle) to the analyser, and photoelectrons were measured at an emission angle of 0° to the surface normal. Survey spectra were acquired using a pass energy of 80 eV, with one sweep at a 0.5 eV step size, and 300 ms dwell time. High-resolution narrow scans of the B 1s, N 1s, and C 1s core levels were acquired using a pass energy of 20 eV, a 0.1 eV step size, and 200 ms dwell time. Repeat sweeps of narrow scans were acquired until either a signal-to-noise ratio of 200 or a maximum of 10 sweeps was reached. Due to the electrically insulating nature of the hBN samples, a charge neutraliser (*i.e.* a low-energy electron flood source) was switched on during the measurement to mitigate surface charging. All spectra were subsequently energy referenced to the C–C chemical component of the C 1s core level at 285.0 eV.

CasaXPS software (version 2.3.25)[20] was used to measure selected peak areas with the NPL transmission function (intensity) calibration[21] and average matrix relative sensitivity factors[22] to determine the concentrations of the detectable elements present. A Tougaard-type or a linear background was used to remove the intensity contribution from the inelastic secondary electrons.[23]

Irradiation tests. The irradiation of the hBN samples was carried out at the University of Manchester Dalton Cumbrian Facility using a self-contained Foss Therapy Services Model 812 ^{60}Co gamma irradiator.[24] Both printed hBN films and membranes were placed into clear 20 mL borosilicate vials for irradiation. Samples were irradiated in two batches under different conditions: in the first batch, the printed samples were crimp-sealed and purged with argon to remove both moisture and oxygen from the vial atmosphere, whilst the membranes were irradiated in moisture-free air obtained by purging sealed samples with synthetic air. The vials were stored after irradiation in inert condition and were opened immediately before the Raman measurements to minimize any possible change in structure due to air exposure. The samples were then subsequentially measured by XPS.

In the second batch, *ca.* 0.1 mL of deionised water was added to each vial to perform irradiation tests in presence of water. The samples were then crimp-sealed under aerated condition, hence reaching a relative humidity (RH) of *ca.* 95% on saturation. Note that the samples were not in direct contact with water during sample preparation and irradiation: the droplet of water was placed in the corner of the vial, while the hBN samples were tilted to land in the dry corner of the same vial.

Irradiations were carried out at an average dose rate of 160 ± 26 Gy min^{-1}. Both batches received a total absorbed doses of 250 kGy, 500 kGy, 750 kGy, 1000 kGy, and 1500 kGy, as verified by Fricke dosimetry.[25] This exposure duration was chosen to simulate high-absorbed dose radiation environments, such as those encountered in space missions, nuclear reactors, or radiation shielding in medical devices, where materials may be exposed to intense radiation over relatively short periods.

3. Results and discussion

Fig. 1a shows the optical pictures of a representative hBN dispersion and membrane, while Fig. 1b shows a representative profile of the printed hBN made with 60 PPs, taken by profilometry. The inset in Fig. 1c shows the printed hBN lines on silicon made with different numbers of PPs. Fig. 1c shows the relation between the printed film thickness and the number of PPs, where the error bars are the RMS roughness measured for each film. The linear fit of this data shows that the thickness of the printed hBN films increases by 13 nm for each PP. The hBN membrane has thickness of ~700 μm, as observed by optical microscopy.

Fig. 1d shows the optical pictures of the hBN membrane before and after exposure to γ-radiation: the irradiation treatment results in the yellowing of the cellulose substrate, in contrast to the hBN film that does not show appreciable change in colour. Table 1 shows a summary of all the prepared samples and irradiation conditions used.

3.1 Irradiation tests in water-free conditions

Raman spectroscopy is a powerful tool for analysing the properties of graphene and 2D materials.[26–28] The spectrum of

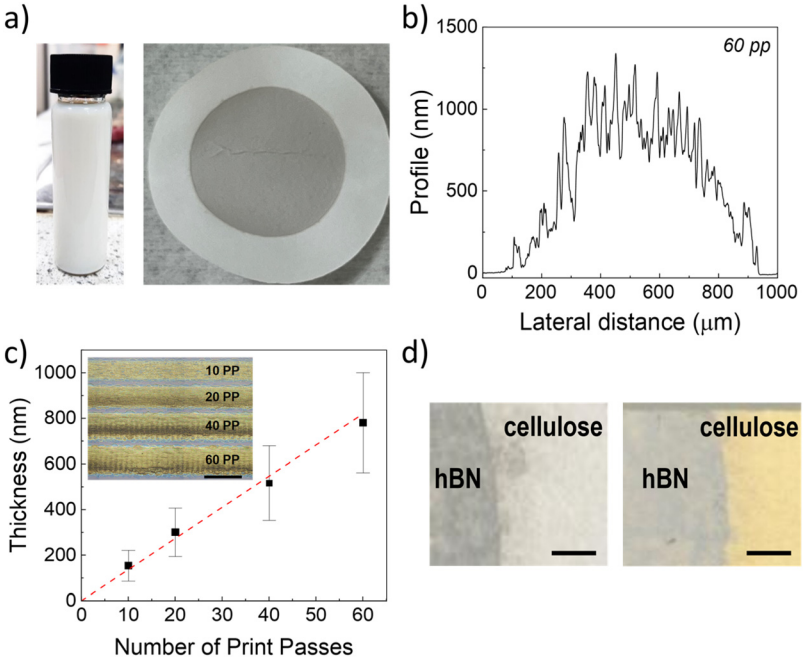

Fig. 1 (a) Optical images of the as-prepared hBN dispersion and the hBN membrane on the cellulose filter. (b) Profile of the printed hBN line made with 60 PPs obtained by profilometry. (c) Thickness of the printed hBN lines *versus* number of PPs. Inset: optical pictures of the printed lines made at different PPs. Scale bar = 500 μm. (d) Optical image of the hBN membrane on the filter before (left) and after (right) irradiation (dose: 1000 kGy). Scale bar = 1 mm. Irradiations were carried out at an average dose rate of 160 ± 26 Gy min^{-1}.

Table 1 Summary of types of hBN samples, γ-ray radiation absorbed doses and atmospheric conditions used in this work. Irradiations were carried out at an average dose rate of 160 ± 26 Gy min^{-1}

Batch number	Type of sample	Conditions during irradiation	γ-Ray absorbed dose (kGy)
1	Printed film	Argon (0% RH)	250, 500, 750, 1000 and 1500
	Membrane	Dry air (0% RH)	
2	Printed film	Ambient (~95% RH)	
	Membrane	Ambient (~95% RH)	

hBN typically features a single peak at 1365 cm^{-1}, which is the equivalent of the G-peak of graphite, *i.e.* it corresponds to the E_{2g} vibrational mode of the B–N atoms of hBN.[29–31] Fig. 2a shows the Raman spectra of the pristine and irradiated hBN membranes from the first batch of samples that were irradiated in water-free conditions. Visual inspection of Fig. 2a shows no appreciable changes in position or shape, even up to the higher absorbed doses. Fig. 2b–d shows representative Raman spectra of the as-printed and irradiated hBN films made with increasing number of PPs (additional Raman spectra of the printed hBN films are available in the ESI, Fig. S1 and S2†). A summary of the average peak position and average FWHM is provided in Tables S1 and S2.† One can see that the hBN Raman peak is not affected by either the film thickness or irradiation absorbed dose. Note that small variations in the position have been observed when moving from few layers to single layer hBN,[30] due to the doping/strain effect from the substrate.[32] However, in our case the films and membranes have thickness above 100 nm and are made by stacking multi-layer nanosheets, so these effects can be excluded. Furthermore, the Raman measurements on the printed films at increasing thickness allow us to exclude any major effect on the film structure coming from indirect interaction of the γ-rays with the silicon substrate, *i.e.* by the absorbed energy or charge or reactive radicals accumulated in the silicon upon irradiation that could be subsequentially transferred to the hBN film.

To better evaluate changes in the structure due to the irradiation, the hBN Raman peaks were fitted with a Lorentzian lineshape (red lines in Fig. 2) and their position and FWHM analysed as a function of the absorbed dose. Fig. 3a and b show the peak position and FWHM of the hBN peak measured on the pristine and irradiated membranes: the position remains stable at ~1367 cm^{-1} as well as the FWHM (~15 cm^{-1}), up to the maximum absorbed dose. These results demonstrate that the hBN structure is not affected by the interaction with the γ-rays. Fig. 3c and d show the peak position and FWHM of the hBN peak measured on the pristine and irradiated films made with different PPs, with variations within spectral resolution of the spectrometer (2–3 cm^{-1}) The

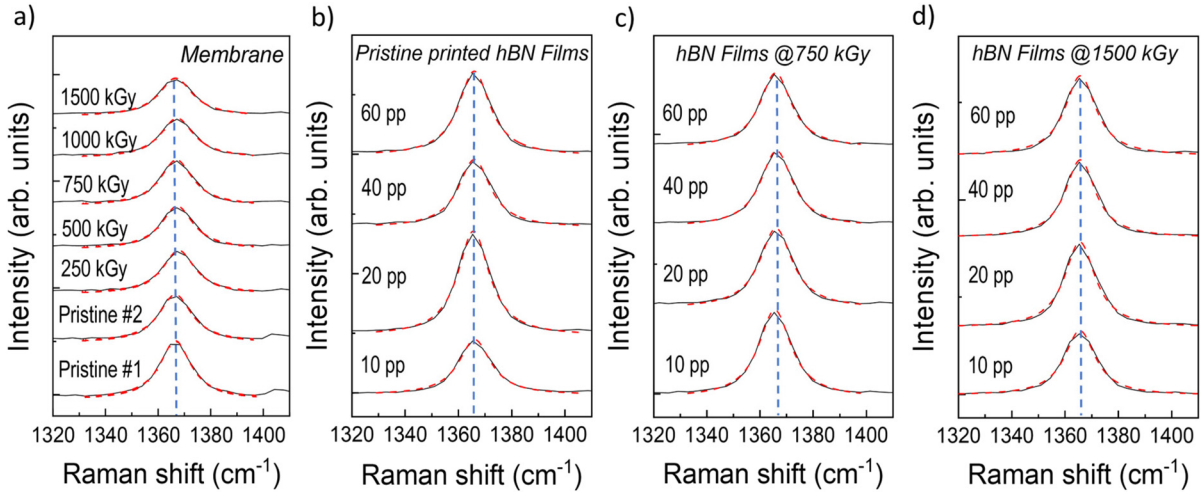

Fig. 2 Representative Raman spectra of: (a) the pristine and irradiated membranes from batch 1; (b) pristine printed hBN films; (c) printed hBN films irradiated at 750 kGy from batch 1; and (d) printed hBN films irradiated at 1500 kGy from batch 1. The dashed lines are a visual guide to show the peak position of hBN. Irradiations were carried out at an average dose rate of 160 ± 26 Gy min^{-1}.

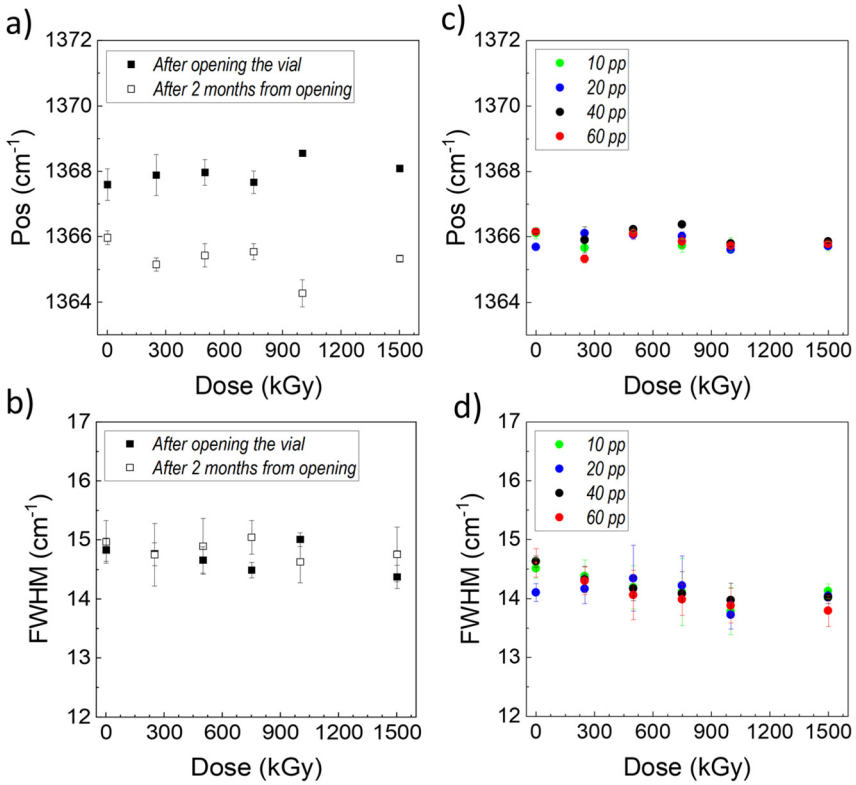

Fig. 3 (a) Position and (b) FWHM of the hBN Raman peak with their standard deviation measured on the membranes from batch 1 as a function of absorbed dose, measured immediately after opening the vials (filled markers) and after two months from opening (open markers). (c) Position and (d) the FWHM with their standard deviation of the hBN peak measured on printed hBN lines made with different PPs, subjected to γ-rays. Irradiations were carried out at an average dose rate of 160 ± 26 Gy min^{-1}.

average peak position is ~1366 cm^{-1} and the average FWHM is ~14 cm^{-1}.

To examine the possibility of the irradiated hBN membranes to develop structural changes after exposure to air, caused by possible defect formation or functionalization of the material, additional measurements were conducted after storage of the membranes in air for two-months. Fig. 3a and b compare the Raman fit parameters of the membranes right

after opening the vials (filled markers) and after two months (open markers). The hBN peak position shows a decrease in position of ~2–3 cm^{-1}, which is however within the spectrometer's resolution, while the FWHM does not change, hence significant changes in the structure following exposure to air after irradiation can be excluded – note that defects formation would lead to changes in both hBN peak FWHM and position. A possible explanation for the small change in peak position after prolonged air exposure could be related to doping of the hBN film from adsorption of water molecules from the humidity. While hBN is hydrophobic, the hBN nanosheets used in these study are functionalised with the PS1 molecule, used as stabilizer,[33] hence enabling water adsorption onto the hBN film.[34]

To support the Raman results and assess the elemental and chemical composition of the hBN before and after irradiation, XPS measurements were also performed on selected hBN membranes. Fig. 4a shows a representative survey spectrum of the hBN sample irradiated at an absorbed dose of 1500 kGy.

The main photoelectron peaks are annotated, *i.e.* O 1s, N 1s, C 1s, B 1s, and the Si 2p core levels, along with the O and N Auger features, *i.e.* O KLL and N KLL peaks. Fig. S3 in the ESI† shows the representative survey spectra from the selected samples from the first batch. The average homogeneous-equivalent atomic composition of each sample is shown in Table 2.

The ratio of the atomic fraction between B and N is within 5% of unity for all samples, indicating that no stoichiometric changes of the hBN have occurred with irradiation, in agreement with the Raman spectroscopy results. Fig. 4b and c show high-resolution spectra of the N 1s and B 1s core levels respectively, acquired from hBN samples irradiated with an absorbed dose of 500 kGy, 1000 kGy, and 1500 kGy, including a non-irradiated sample. Both the B 1s and N 1s peaks for all samples predominately exhibit a single component. On the pristine sample, the N 1s peak is observed at 398.3 eV and the B 1s peak is observed at 190.7 eV on the binding energy scale. For the irradiated samples, both the N 1s and B 1s peaks exhibit a shift of 0.2 eV to lower binding energies. The binding energy difference between the N 1s and B 1s is consistent for all measured samples (*i.e.*, 207.6 ± 0.1 eV on average, ESI, Table S3†), so the 0.2 eV shift observed between the pristine and irradiated samples is not due to chemical differences but is instead attributed to surface charging differences, possibly caused by changes in the substrate or film chemical composition after exposure to γ-rays, rather than the hBN. Even with the surface charging induced rigid shifts, the binding energies of all the N 1s and B 1s core levels are indicative of nitrogen bonded to boron. The stoichiometric ratios from the survey spectra and binding energy positions of the B 1s and N 1s peaks thus confirm the presence of BN and confirm that no

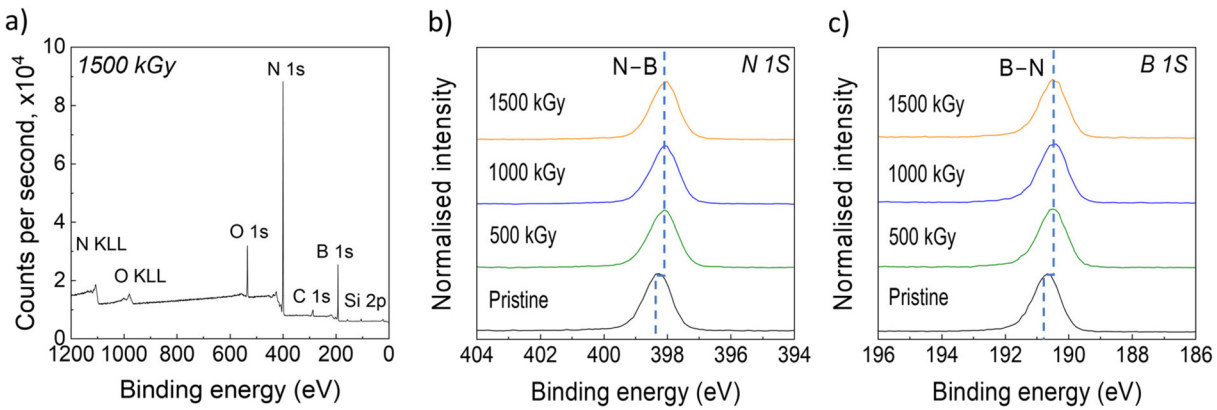

Fig. 4 XPS spectra acquired on the pristine and irradiated hBN membranes from the first batch. (a) A survey spectrum of the 1500 kGy irradiated hBN membrane annotated with the detected core levels used for quantification. The Auger peaks for oxygen and nitrogen are also shown. High-resolution spectra of (b) N 1s and (c) B 1s core levels from 500 kGy, 1000 kGy, and 1500 kGy irradiated hBN membranes including a pristine sample that has not been irradiated. Irradiations were carried out at an average dose rate of 160 ± 26 Gy min^{-1}.

Table 2 Average homogeneous-equivalent atomic composition of pristine (control) and irradiated hBN membranes at 500, 1000 and 1500 kGy from batch 1. The average B/N ratio for each sample is also shown with expanded uncertainty (coverage factor, *k*, of 2)

		Atomic composition (atomic%)					
Sample	Irradiation absorbed dose/kGy	B	N	C	O	Si	B/N ratio ± uncertainty (k = 2)
hBN membranes	Pristine	29.6	28.6	25.6	16.0	0.2	1.04 ± 0.07
	500	31.4	30.4	21.2	16.9	0.1	1.03 ± 0.07
	1000	42.8	42.3	7.0	7.2	0.7	1.01 ± 0.08
	1500	43.6	42.6	5.3	7.2	1.2	1.02 ± 0.08

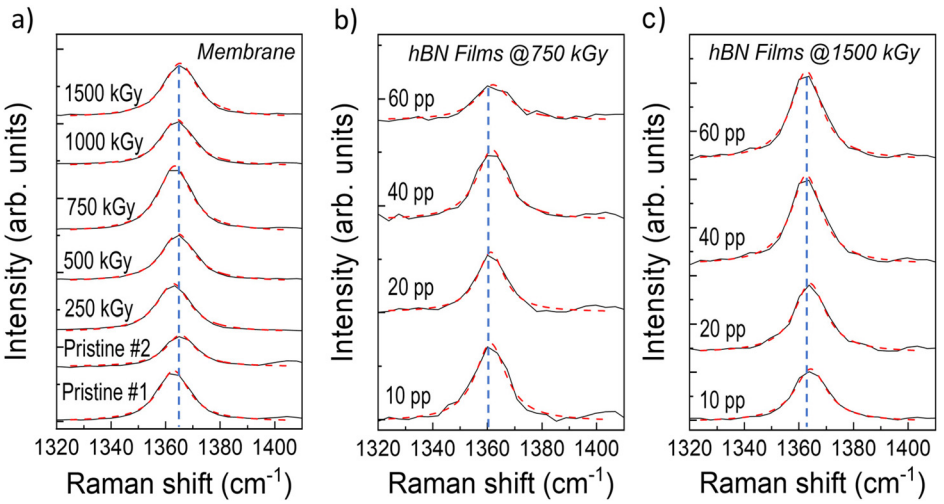

Fig. 5 Representative Raman spectra of the pristine and irradiated membranes from batch 2; (a) hBN membranes irradiated at different doses; (b) printed hBN films irradiated at 750 kGy under inert conditions; and (c) printed hBN films irradiated at 1500 kGy under inert conditions. The dashed lines are a visual guide to show the peak position of hBN. Irradiations were carried out at an average dose rate of 160 ± 26 Gy min^{-1}.

chemical changes have occurred in the hBN membrane samples during irradiation.

XPS also indicates a small decrease in the C/O ratio with increasing absorbed dose, suggesting a possible small reduction of the organic residual from the printable solvent, which is expected to be more susceptible to radiolysis than hBN, as observed for carbon nanotubes,[35] *i.e.* the organic residual is likely to be more subjected to radiation-induced charge and energy transfer from hBN, which gets charged upon irradiation. In addition, hBN can catalyse oxidation reactions of aliphatic organics,[36–38] so hBN may accelerate the degradation of residual organics through a combination of radiolysis and catalytic oxidation. Finally, a further explanation may be given by the degradation of the cellulose substrate upon irradiation, with possible release of CH_4 permeating in the hBN membrane.[39]

3.2 Irradiation tests in presence of water

To investigate any possible effect on the radiation tolerance of both printed films and membranes in the long-term environmental stability, γ-rays irradiation tests were conducted under more realistic (*i.e.* closer to the environment found in applications) ambient conditions.

Fig. 5a illustrates the Raman spectra of the pristine and irradiated hBN membranes at high RH: visual inspection does not show any noticeable changes in the spectra. Fig. 5b and c show representative Raman spectra of the printed films irradiated at absorbed doses of 750 kGy and 1500 kGy with increasing number of PPs (additional Raman spectra of printed hBN films are available in the ESI, Fig. S4 and S5†). A summary of the average peak position and average FWHM is provided in Tables S4 and S5.† No appreciable changes in the hBN Raman peak are observed with increasing number of PPs.

Fig. 6a and b show the peak position and FWHM of the hBN peak measured on the pristine and irradiated membranes: the position remains stable at ~1364 cm^{-1} and FWHM at ~14 cm^{-1}, up to the maximum absorbed dose. Remarkably, this value is very close to the one measured for the membrane irradiated in water-free condition but measured after 20 days of exposure in air (Fig. 3a). This seems to confirm that the difference in peak position observed in Fig. 3a should be attributed to doping, i.e. to charge transfer from water molecules adsorbed onto the hBN nanosheets.

Fig. 6c and d show the peak position and FWHM of the hBN peak measured on the pristine and irradiated printed films made with different PPs. The average peak position of hBN is ~1364 cm^{-1} and the average of FWHM is ~14 cm^{-1}, comparable to the one measured on the pristine and irradiated membranes under the same conditions considering the spectrometer's resolution (~2–3 cm^{-1}). Note that there is a relatively strong variation in the peak position of the printed hBN films in contrast to Fig. 3c – this could be attributed doping from the water adsorbed to the films, as the samples have not been sealed after irradiation, so they have been exposed to air for several days before taking the Raman measurements.

Fig. S6a† shows a representative survey spectrum acquired from a hBN sample irradiated at an absorbed dose of 1500 kGy from the second batch. The main photoelectron peaks are annotated, *i.e.* O 1s, N 1s, C 1s, B 1s, and the Si 2p core levels, along with the O and N Auger features, *i.e.* O KLL and N KLL peaks. More survey spectra of the second batch of samples can be found in the ESI (see Fig. S7†). Table 3 indicates the average homogenous-equivalent atomic composition of each hBN membrane. The ratio of the atomic fraction between B and N is within 5% of unity for all samples as shown in Table 2, indicating that no stoichiometric changes of the hBN have occurred with irradiation, in agreement with the previous results (Fig. 4 and Table 2).

Fig. S6b and S6c† show high-resolution spectra of the N 1s and B 1s core levels respectively, acquired from hBN samples

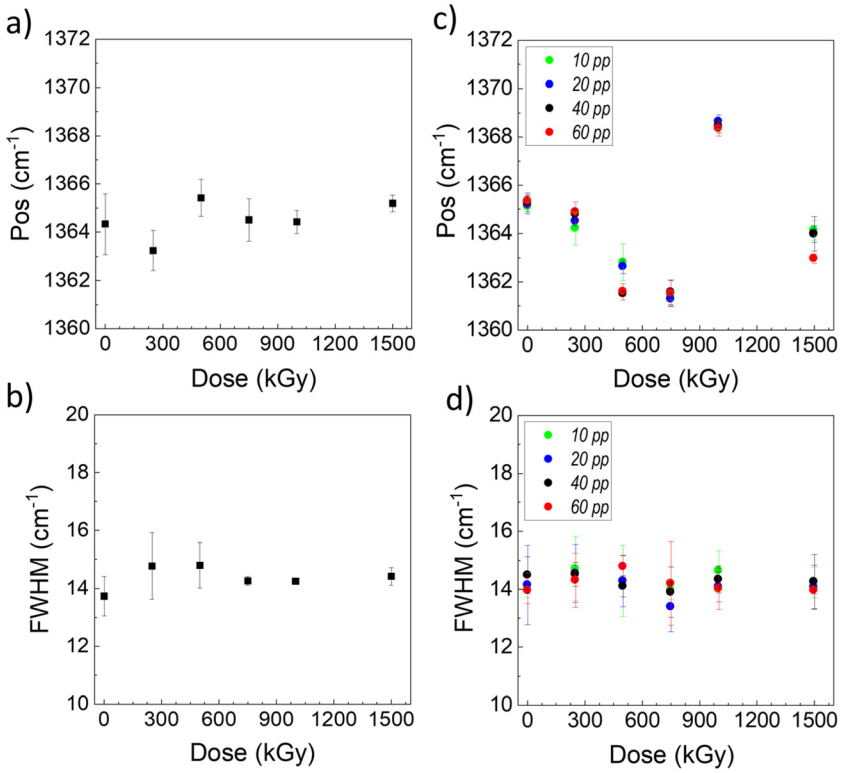

Fig. 6 Comparison of the Raman fitting parameters, (a) position and (b) FWHM of the hBN membranes as function of the irradiation absorbed doses. The Raman fitting parameters, (c) position and (d) the FWHM of the printed hBN lines at different PPs (10, 20, 40 and 60) for increasing absorbed dose under ambient conditions.

Table 3 Average homogeneous-equivalent atomic composition of pristine (control) and irradiated hBN membranes at high RH (batch 2). The average B/N ratio for each sample is also shown with expanded uncertainty (coverage factor, *k*, of 2)

		Atomic composition (atomic%)					
Sample	Irradiation absorbed dose/kGy	B	N	C	O	Si	B/N ratio ± uncertainty (k = 2)
hBN membranes	Pristine	30.9	29.8	23.4	15.4	0.0	1.04 ± 0.07
	250	45.0	43.7	7.2	4.1	0.0	1.03 ± 0.08
	500	45.1	44.0	6.6	4.3	0.0	1.03 ± 0.08
	750	27.4	26.1	23.7	22.9	0.0	1.05 ± 0.06
	1000	32.7	31.8	18.1	17.4	0.0	1.03 ± 0.07
	1500	39.7	39.0	10.1	11.2	0.0	1.02 ± 0.08

irradiated with an absorbed dose of 250, 500, 700, 1000 and 1500 kGy, and a non-irradiated control sample. Both the B 1s and N 1s peaks for all samples predominately exhibit a single component. On the pristine sample, the N 1s peak is observed at 398.3 eV and the B 1s peak is observed at 190.7 eV on the binding energy scale. For the irradiated samples, both the N 1s and B 1s peaks exhibit a small shift of ~0.2 eV to lower binding energies. The binding energy difference between the N 1s and B 1s is consistent for all measured samples (*i.e.*, 207.6 ± 0.4 eV on average), again, despite the surface charging induced shifts, our results on the second batch of irradiated hBN membrane samples yield similar results to the first batch, *i.e.* single component B 1s and N 1s peaks, consistent binding energy differences and a B/N ratio within 5% of unity, as shown in Table 3 and Table S6 in the ESI,† confirming that the hBN structure is unaffected by γ-ray radiation up to 1500 kGy.

Notably, we observed the presence of silicon when the XPS measurements were performed for the second batch of hBN membrane samples, in contrast to the results obtained in first batch (Table 2). This could be due to unintentional contamination (*e.g.* silicon-based greases) during sample handling.

Table 3 shows a decrease in the C/O ratio with increasing absorbed dose, although the changes with absorbed dose are different from those observed for batch 1 samples (Table 2). This is likely due to the presence of water during irradiation: the film is hydrophobic,[34] so water is likely to get adsorbed in the membrane during irradiation and will participate in the

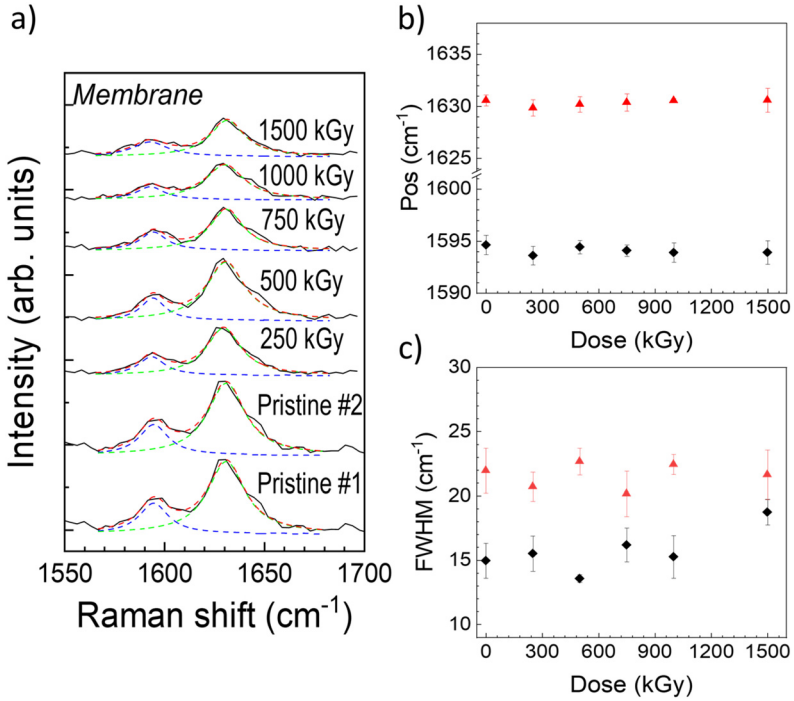

Fig. 7 (a) Representative Raman spectra of the pristine and irradiated membranes from batch 2. (b) Peak position and (c) FWHM of the carbon peaks located at ~1595 cm^{-1} and ~1630 cm^{-1}, as a function of the absorbed dose. Irradiations were carried out at an average dose rate of 160 ± 26 Gy min^{-1}.

radiolysis. Water may also accelerate degradation of cellulose to CH_4.[39]

To further investigate any change in the organic residual signal with the absorbed dose. Raman spectroscopy was also performed on the C–C region (1500–1700 cm^{-1}).

Fig. 7a shows representative Raman spectra of the pristine and irradiated membranes in the carbon region. We observed two peaks located at ~1595 cm^{-1} and ~1630 cm^{-1}, respectively, which remain present even up to the highest irradiation absorbed doses of 1500 kGy. A summary of the average peak position and average FWHM is provided in Table S7.† These peaks correspond to C=C stretching modes,[40,41] and they are quite broad, so they are associated with a disordered carbon-based residual, for example from the pyrene derivative used as a stabilizer and the Triton-X used for the printable solvent (see methods). The position and FWHM of both peaks, measured for the pristine and irradiated membranes, are presented in Fig. 7b and c. The results clearly indicate that the average position and FWHM of both peaks remain stable at ~1595 cm^{-1} and ~1630 cm^{-1} across all irradiation absorbed doses, indicating no appreciable structural change in the organic residual in the film upon γ-irradiation. This seems to be in contrast with the XPS results, which show a change in the C/O ratio – however, due to the disordered nature of the organic residual, Raman spectroscopy may not be able to detect small changes in the C/O ratio. Furthermore, additional effects coming from the degradation from the cellulose membrane, upon radiolysis, could play a role that may not be detectable by Raman spectroscopy.

4. Conclusion

In this work we have investigated the γ-radiation tolerances (up to 1500 kGy) of films made by liquid phase exfoliated hBN nanosheets in water, deposited by inkjet printing and vacuum filtration. Our results show no appreciable change in the hBN structure after irradiation no matter the thickness of the film, the deposition method and the environment studied. Our results are in contrast to those obtained in ref. 8, which shows changes in the structure, including phase changes and oxidation, at absorbed doses much smaller than the ones used in our work. The discrepancy may be due to the use of a different material type and preparation methods. In particular, our hBN nanosheets are functionalised with a pyrene derivative and the printable solvent contains organic additives, which may protect the nanosheets from oxidation, as observed for other air-sensitive nanosheets produced by LPE.[42] The organic additive may also be responsible for the excellent resistance to γ-ray as it could serve as a "sacrificial lamb" to radiolytic degradation, either by radical trapping and/or energy/charge transfer from the irradiated hBN nanosheets to the organic impurities.

In conclusion, the remarkable radiation resistance and environmental durability of films and membranes made by solution-processed hBN make them promising candidates as coatings and thin films for the nuclear and space industry, as they are able to retain their physical, chemical and mechanical properties without degrading upon γ-ray exposure.

Author contributions

The project was conceived and designed by C. C. The films were printed and characterised by profilometry by T. I. A. J. W. performed most of the Raman measurements and related analysis. Additional measurements were performed by Y. A. and T. A. The hBN ink was produced by Z. P. The membranes were produced by K. P. W. L. and B. P. R. performed XPS and related analysis under the supervision of A. J. P. A. B. performed and supervised the irradiation experiments. The manuscript has been written by J. W. and C. C. with contributions from all authors.

Conflicts of interest

There are no conflicts to declare.

Data availability

The data supporting this article (representative Raman spectra and average and standard deviations of the Raman fit parameters discussed in this work) have been included in both the main text and the ESI.†

Acknowledgements

TIA and CC acknowledge the Nuclear Decommission Authority for funding this project. ZP thanks the CSC for financial support. KP and YA acknowledge support from the UKRI (grant EP/X028844/1). AB acknowledges the support of The University of Manchester's Dalton Cumbrian Facility (DCF), a partner in the National Nuclear User Facility, the EPSRC UK National Ion Beam Centre and the Henry Royce Institute. CC acknowledges the National Graphene Institute at Manchester for access to the Raman spectrometer. JW, WL, BPR and AJP acknowledge support from the National Measurement System (NMS) of the Department for Science, Innovation and Technology (DSIT), UK, (project # 128807).

References

1 K. S. Novoselov, V. I. Fal'ko, L. Colombo, P. R. Gellert, M. G. Schwab and K. Kim, *Nature*, 2012, **490**, 192–200.
2 A. C. Ferrari, F. Bonaccorso, V. Fal'ko, K. S. Novoselov, S. Roche, P. Bøggild, S. Borini, F. H. L. Koppens, V. Palermo, N. Pugno, J. A. Garrido, R. Sordan, A. Bianco, L. Ballerini, M. Prato, E. Lidorikis, J. Kivioja, C. Marinelli, T. Ryhänen, A. Morpurgo, J. N. Coleman, V. Nicolosi, L. Colombo, A. Fert, M. Garcia-Hernandez, A. Bachtold, G. F. Schneider, F. Guinea, C. Dekker, M. Barbone, Z. Sun, C. Galiotis, A. N. Grigorenko, G. Konstantatos, A. Kis, M. Katsnelson, L. Vandersypen, A. Loiseau, V. Morandi, D. Neumaier, E. Treossi, V. Pellegrini, M. Polini, A. Tredicucci, G. M. Williams, B. Hee Hong, J.-H. Ahn, J. Min Kim, H. Zirath, B. J. van Wees, H. van der Zant, L. Occhipinti, A. Di Matteo, I. A. Kinloch, T. Seyller, E. Quesnel, X. Feng, K. Teo, N. Rupesinghe, P. Hakonen, S. R. T. Neil, Q. Tannock, T. Löfwander and J. Kinaret, *Nanoscale*, 2015, **7**, 4598–4810.
3 M. J. Molaei, M. Younas and M. Rezakazemi, *ACS Appl. Electron. Mater.*, 2021, **3**, 5165–5187.
4 K. K. Kim, H. S. Lee and Y. H. Lee, *Chem. Soc. Rev.*, 2018, **47**, 6342–6369.
5 K. Zhang, Y. Feng, F. Wang, Z. Yang and J. Wang, *J. Mater. Chem. C*, 2017, **5**, 11992–12022.
6 A. E. Naclerio and P. R. Kidambi, *Adv. Mater.*, 2023, **35**, 2207374.
7 P. Li, W. Cheng, Y. Zhou, D. Zhao, J. Liu, L. Li, X. Ouyang, B. Liu, W. Jia, Q. Xu and K. (Ken) Ostrikov, *Adv. Mater.*, 2023, **35**, 2209452.
8 H. Khan, I. Ahmad, T.-K. Zhao, F. Sparis, S. S. Hussain, A. Diallo, J. Iqbal, F. I. Ezema, M. Ikram, M. Malik, M. Z. Khan, S. Ilyas and T. Jan, *Mater. Res. Express*, 2019, **6**, 1150b2.
9 L. Jiao, Y. Wang, Z. Wu, H. Shen, H. Weng, H. Chen, W. Huang, M. Wang, X. Ge and M. Lin, *Polym. Degrad. Stab.*, 2021, **190**, 109643.
10 E. Cazalas, M. R. Hogsed, S. Vangala, M. R. Snure and J. W. McClory, *Appl. Phys. Lett.*, 2019, **115**, 223504.
11 A. G. Kelly, D. O'Suilleabhain, C. Gabbett and J. N. Coleman, *Nat. Rev. Mater.*, 2021, **7**, 217–234.
12 S. Conti, G. Calabrese, K. Parvez, L. Pimpolari, F. Pieri, G. Iannaccone, C. Casiraghi and G. Fiori, *Nat. Rev. Mater.*, 2023, **8**, 651–667.
13 D. McManus, S. Vranic, F. Withers, V. Sanchez-Romaguera, M. Macucci, H. Yang, R. Sorrentino, K. Parvez, S.-K. Son, G. Iannaccone, K. Kostarelos, G. Fiori and C. Casiraghi, *Nat. Nanotechnol.*, 2017, **12**, 343–350.
14 C.-X. Hu, Y. Shin, O. Read and C. Casiraghi, *Nanoscale*, 2021, **13**, 460–484.
15 R. Worsley, L. Pimpolari, D. McManus, N. Ge, R. Ionescu, J. A. Wittkopf, A. Alieva, G. Basso, M. Macucci, G. Iannaccone, K. S. Novoselov, H. Holder, G. Fiori and C. Casiraghi, *ACS Nano*, 2019, **13**, 54–60.
16 M. Rahman, K. Parvez, G. Fugallo, C. Dun, O. Read, A. Alieva, J. Urban, M. Lazzeri, C. Casiraghi and S. Pisana, *Nanomaterials*, 2022, **12**, 3861.
17 O. Read, Y. Shin, C. Hu, M. Zarattini, M. Boyes, X. Just-Baringo, A. Panigrahi, I. Larrosa and C. Casiraghi, *Carbon*, 2022, **186**, 550–559.
18 H. Yang, F. Withers, E. Gebremedhn, E. Lewis, L. Britnell, A. Felten, V. Palermo, S. Haigh, D. Beljonne and C. Casiraghi, *2D Mater.*, 2014, **1**, 011012.
19 A. C. Ferrari and J. Robertson, *Phys. Rev. B: Condens. Matter Mater. Phys.*, 2001, **64**, 075414.
20 N. Fairley, V. Fernandez, M. Richard-Plouet, C. Guillot-Deudon, J. Walton, E. Smith, D. Flahaut, M. Greiner, M. Biesinger, S. Tougaard, D. Morgan and J. Baltrusaitis, *Appl. Surf. Sci. Adv.*, 2021, **5**, 100112.

21 M. P. Seah, M. Suzuki, K. Doumae and A. Tanaka, *J. Surf. Anal.*, 2022, **28**, S33–S46.
22 M. Seah, I. Gilmore and S. Spencer, *J. Electron Spectrosc. Relat. Phenom.*, 2001, **120**, 93–111.
23 S. Tougaard, *J. Vac. Sci. Technol., A*, 2021, **39**, 1011201.
24 L. Leay, A. Baidak, C. Anderson, C. M. Chan, A. Daubney, T. Donoclift, G. Draper, R. Edge, J. Hobbs, L. Jones, N. J. S. Mason, D. Messer, M. O'Leary, R. Orr, S. M. Pimblott, S. de Moraes Shubeita, A. D. Smith, H. Steele, P. Wady and F. Currell, *Appl. Sci.*, 2021, **11**, 11081.
25 J. W. Mullin, *Crystallization*, 2001.
26 A. Jorio, R. Saito, G. Dresselhaus and M. S. Dresselhaus, *Raman Spectroscopy in Graphene Related Systems*, Wiley, 2011.
27 C. Casiraghi, in *Spectroscopic Properties of Inorganic and Organometallic Compounds*, 2012, vol. 43, pp. 29–56.
28 A. C. Ferrari and D. M. Basko, *Nat. Nanotechnol.*, 2013, **8**, 235–246.
29 I. Stenger, L. Schué, M. Boukhicha, B. Berini, B. Plaçais, A. Loiseau and J. Barjon, *2D Mater.*, 2017, **4**, 031003.
30 R. V. Gorbachev, I. Riaz, R. R. Nair, R. Jalil, L. Britnell, B. D. Belle, E. W. Hill, K. S. Novoselov, K. Watanabe, T. Taniguchi, A. K. Geim and P. Blake, *Small*, 2011, **7**, 465–468.
31 R. Arenal, A. C. Ferrari, S. Reich, L. Wirtz, J.-Y. Mevellec, S. Lefrant, A. Rubio and A. Loiseau, *Nano Lett.*, 2006, **6**, 1812–1816.
32 Q. Cai, D. Scullion, A. Falin, K. Watanabe, T. Taniguchi, Y. Chen, E. J. G. Santos and L. H. Li, *Nanoscale*, 2017, **9**, 3059–3067.
33 K. Parvez and C. Casiraghi, *Acc. Chem. Res.*, 2025, **58**, 189–198.
34 L. Chen, K. Hu, M. Lu, Z. Chen, X. Chen, T. Zhou, X. Liu, W. Yin, C. Casiraghi and X. Song, *Adv. Mater.*, 2024, **36**, 1–8.
35 H.-Y. Chao, A. M. Nolan, A. T. Hall, D. Golberg, C. Park, W.-C. D. Yang, Y. Mo, R. Sharma and J. Cumings, *J. Phys. Chem. C*, 2024, **128**, 18328–18337.
36 J. M. Venegas, W. P. McDermott and I. Hermans, *Acc. Chem. Res.*, 2018, **51**, 2556–2564.
37 X. Zhang, R. You, Z. Wei, X. Jiang, J. Yang, Y. Pan, P. Wu, Q. Jia, Z. Bao, L. Bai, M. Jin, B. Sumpter, V. Fung, W. Huang and Z. Wu, *Angew. Chem., Int. Ed.*, 2020, **59**, 8042–8046.
38 J. M. Venegas, Z. Zhang, T. O. Agbi, W. P. McDermott, A. Alexandrova and I. Hermans, *Angew. Chem., Int. Ed.*, 2020, **59**, 16527–16535.
39 N. Bleyen, V. Van Gompel, S. Smets, S. Eyley, W. Verwimp, W. Thielemans and E. Valcke, *Radiat. Phys. Chem.*, 2023, **212**, 111177.
40 D. S. Cordeiro and P. Corio, *J. Braz. Chem. Soc.*, 2009, **20**, 80–87.
41 X. Gu, S. Tian, Q. Zhou, J. Adkins, Z. Gu, X. Li and J. Zheng, *RSC Adv.*, 2013, **3**, 25989.
42 L. Niu, J. N. Coleman, H. Zhang, H. Shin, M. Chhowalla and Z. Zheng, *Small*, 2016, **12**, 272–293.